Effect of Char Loading on Reduction Kinetics of Cu-Based Oxygen Carriers in a Drop-Tube Fluidized Bed Reactor at Temperatures from 850° C to 1100° C: Experiment and CFD Modeling

Ward A. Burgess,[,a,b] Nicholas C. Means,[a,b] Bret H. Howard,[a] Mark W. Smith,[c] Dushyant Shekhawat[c]*

[a] National Energy Technology Laboratory, United States Department of Energy, 626 Cochrans Mill Road, Pittsburgh, PA 15236, USA

[b] Leidos Research Support Team, 626 Cochrans Mill Road, PO Box 10940, Pittsburgh, PA 15236, USA

[c] National Energy Technology Laboratory, United States Department of Energy, 3610 Collins Ferry Road, Morgantown, WV 26507, USA

*Corresponding Author: E-mail: Ward.Burgess@NETL.DOE.GOV; Tel: 1-412-386-5409

Abstract

Chemical-looping combustion with oxygen uncoupling (CLOU) is a process using gaseous or solid hydrocarbon fuels and is a promising carbon capture and storage (CCS) technology. In CLOU, combustion of the fuel is achieved through the release of gaseous O_2 from an oxygen carrier material such as CuO and is favored at high temperatures and low O_2 partial pressures. The primary objectives of this study were to (1) compare values for the apparent rate constant $k_{ov}(T)$ for the overall rate of reduction of a CuO carrier, either alone or in the presence of coal char obtained from the pyrolysis of Powder River Basin (PRB) coal, and (2) develop and validate a computational fluid dynamics (CFD) model for the CuO/PRB coal char system based on known kinetics of the individual CuO and Cu_2O reduction, combustion, and gasification reactions. Two oxygen carriers consisting of 20wt% CuO/Al_2O_3 and 9wt% CuO/Al_2O_3 were prepared by physical mixing and by incipient wetness impregnation (IWI), respectively. Kinetic analyses were conducted in the temperature range 850°C-1100°C. The CFD model typically reproduced experimental values of $k_{ov}(T)$ to within ±10%. The increase in $k_{ov}(T)$ caused by addition of only 0.075 gram PRB char per gram CuO was modest at 1100° C, but was more than threefold at 850° C. Combustion and gasification of the coal char produced CO, opening another pathway for CuO reduction in addition to the CLOU reaction, but also resulted in the over-reduction of Cu_2O to the undesired metallic Cu. Production of Cu metal increased with respect to char loading.

Keywords: chemical-looping combustion; computational fluid dynamics; oxygen carrier; copper oxide; solid fuels; fluidized bed reactor

1. Introduction

Arrhenius and Holden hypothesized that increases in atmospheric CO_2 concentration cause the temperature of the earth to rise.[1] Atmospheric CO_2 concentrations may be reduced by carbon capture and storage (CCS). However, the capture of CO_2 from a flue gas mixture remains a difficult and energy intensive task. By replacing air with pure, excess O_2 during fuel combustion in a power plant, the separation of CO_2 from N_2 is no longer necessary. In such a scenario, the gaseous combustion products include only CO_2 and water[2] if combustion is complete.

The reduction of oxygen carriers by the Chemical-Looping Combustion (CLC) process has been studied for the combustion of gaseous fuels such as CH_4/natural gas[3,4] or hydrogen[5] for heat and power production. Because of the abundance of coal as a fuel, previous workers have also investigated CLC of solid fuels, utilizing diverse carbonaceous feedstocks such as coal[6] petroleum coke[6,7] and biomass.[8] The general CLC process is composed of two reactors (Figure 1). An oxygen carrier is reduced, giving off the oxygen needed for fuel combustion in the fuel reactor and then cycled to another reactor where it is re-oxidized by air. Metal oxides of Fe, Ni, Cu, Mn, and Co have been studied as possible oxygen carrier materials. Their application to the CLC process has been reviewed extensively.[9,10] These O_2 carriers are typically prepared on an inert support material such as Al_2O_3, $MgAl_2O_4$, or ZrO_2. There are three types of CLC processes:

(1) syngas-fueled CLC

(2) in situ gasification

(3) Chemical Looping with Oxygen Uncoupling (CLOU)

During syngas-fueled CLC processes the fuel is subjected to gasification, creating syngas which then contacts the carrier and reduces it. When fuel gasification and syngas combustion occur in the same reactor, the process is described as in situ gasification CLC (ig-CLC). The popular, low-cost Fe_2O_3 carrier utilized in syngas-CLC and ig-CLC must react with syngas produced by the gasification reaction if reduction of the carrier is to occur. However, CLOU carriers release oxygen without the need for any other reactant; that is, they undergo auto-reduction (Figure 1). CLOU is desirable because combustion with the O_2 released is considerably faster than gasification kinetics, leading to more than an order-of-magnitude increase in observed CuO reduction rate.[7] The major challenges facing the CLC of solid fuels using Fe_2O_3-based carriers are the slow gasification reaction,[11] ensuring the availability of equilibrium-limited, reversible O_2 transport from CLOU carriers for fuel combustion and the separation of ash and unreacted fuel particles from the metal oxide in all cases.[16] Also the composition of CO in the gas leaving the fuel reactor must be minimized or eliminated.

CLOU eliminates the need for syngas production through gasification while still ensuring the availability of O_2 for combustion of the fuel. Three commonly used CLOU carriers are CuO, Mn_2O_3, and Co_3O_4. These carriers undergo auto-reduction as temperature increases to give off O_2 with no additional reactant needed.[7] Unfortunately, Co_3O_4 has environmental and health issues[7] so it was not considered in this work. The oxidation of Mn_2O_3 in air is thermodynamically limited at temperatures above ~820° C.[7] Notably, 10% of the CuO carrier mass is given off as O_2 during reduction ($4CuO \leftrightarrow 2Cu_2O + O_2$) while only 3% of the Mn_2O_3 carrier mass is given off as O_2 ($6Mn_2O_3 \leftrightarrow 4Mn_3O_4 + O_2$). Previous studies have shown that using CuO as carrier is a promising approach to provide pure gaseous O_2 for solid fuel combustion.[7,12,13,14] For these reasons, CuO was the CLOU carrier used in this work.

The focus of this study is the direct combustion of solid fuels initiated by an equilibrium-limited CLOU type reaction, after which the O_2 liberated reacts with the coal char in a combustion reaction which decreases O_2 concentration and favors further CuO reduction. Many kinetic studies for CuO reduction have been made available,[15] but none of these studies have included comparisons of the observed kinetic rate constants for the equilibrium-limited reduction of CuO both with and without a solid carbon fuel present. While known kinetics for the CLOU, combustion, gasification and reduction reactions have been combined into a comprehensive kinetic model for systems of CuO + gas,[16] to our knowledge no such parallel work has been undertaken for systems of CuO + solid carbon such as coal or coal char.

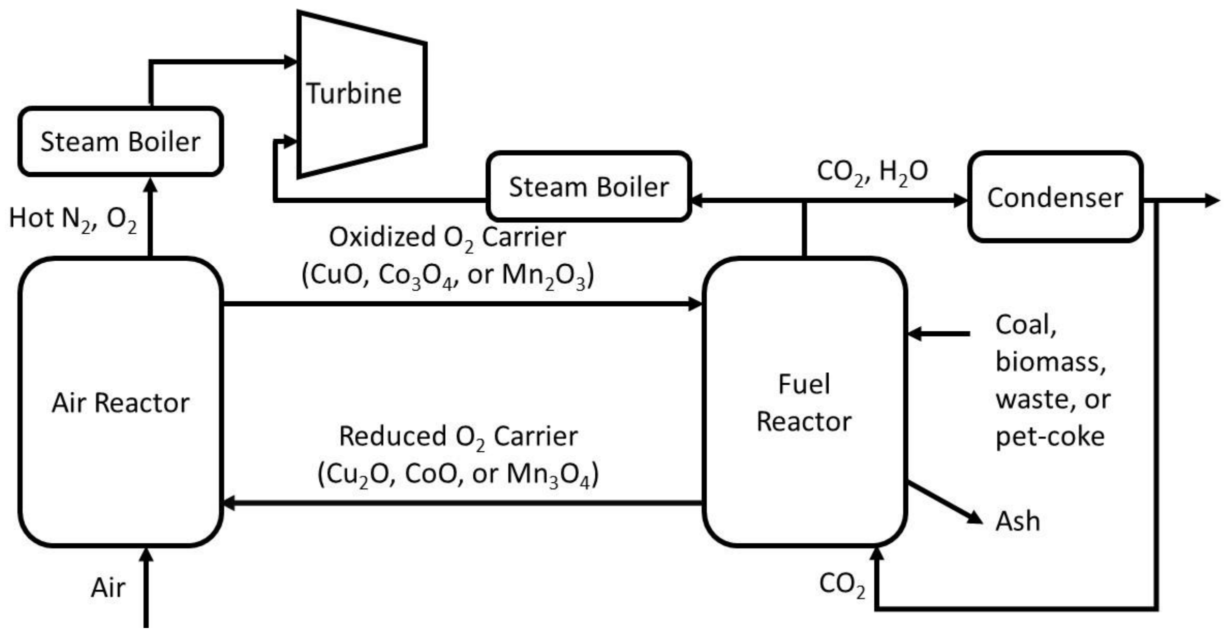

Figure 1. Schematic of a chemical looping with oxygen uncoupling (CLOU) process.

Major reactions occurring in the system of CuO + solid carbon are given in Equations 1-11. A pictorial representation of this reaction system is given in Figure 2. To simplify the modeling and limit the number of reactions occurring in the system, in this work coal char (denoted by C) is considered rather than raw coal. The CLOU reduction reaction for CuO is given in Equation 1. The reaction of C via combustion (Equations 4 and 5) or gasification (Equations 7 and 9) to form CO gas opens alternate CuO reduction pathways (Equations 2 and 3), increasing the overall CuO reduction rate. Kinetic constants of Arrhenius pre-factor and activation energy for the CLOU reaction for CuO-based oxygen carriers were recently reported by our group.[17] Kinetic information for the reduction of CuO by CO is also available.[24] These values could be input to a computational fluid dynamics (CFD) model, which could be used to model the effect of temperature and C:O ratio (mass ratio of char: oxide CuO) on the overall rate of CuO reduction. Unfortunately, the presence of CO gas opens alternate pathways (Equations 3 and 10) for reduction of CuO and Cu_2O to metallic Cu. The Cu metal melts at 1084° C and operating near or above this temperature greatly facilitates agglomeration of the Cu-containing solids in the reactor, leading to loss of fluidization and destroying the effectiveness of the O_2 carrier. To combat agglomeration, the CuO may be deposited onto a support material such as Al_2O_3.[18] Often the process temperature must be set at 900° C or lower[19] even though all reaction kinetics are significantly slower at these conditions than they are at 1084° C. Therefore, it is necessary that a kinetic model accurately predict the conditions under which metallic Cu forms.

In scaled-up CLOU units, the carrier is typically dropped into the fuel reactor to be reduced.[14] In this work, a drop tube fluidized bed reactor (DT-FBR) was used to measure the apparent overall reduction kinetics of CuO-based oxygen carriers under various conditions in the presence of coal char. O_2 carrier reduction kinetic information is critical for the design and operation of CLC reactor systems. To the authors' knowledge, no such kinetic parameters are available in the literature for the reduction of CuO with solid fuel present at temperatures above 1000° C. However, in this study a simple method for determination of the overall apparent kinetic parameters of activation energy and Arrhenius pre-factor for CuO oxygen carrier reduction to Cu_2O in the presence of PRB char at temperatures from 850° C up to 1100° C is presented. These experimental data points are subsequently used to validate a CFD-based kinetic model, which is then used to describe the different reaction pathways by which char addition accelerates the rate of CuO reduction. The effect of char loading magnitude on overall CuO reduction rate is examined. The model is also used to predict the relative quantity of Cu metal that forms at various conditions of temperature and char loading.

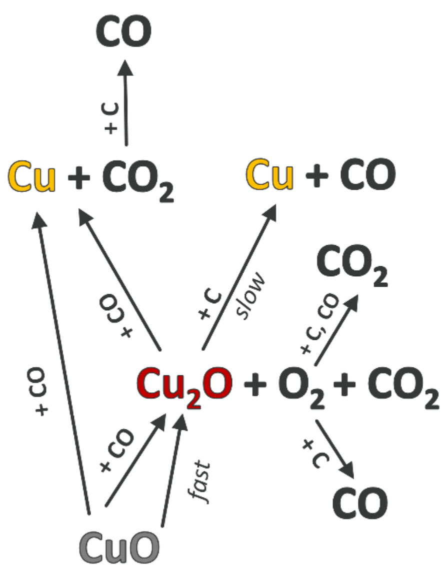

Figure 2. Pictorial representation of the major reactants and species formed when CuO and char (denoted as C) are heated to elevated temperatures 850-1100° C.

$$4CuO \leftrightarrow 2Cu_2O + O_2 \quad (1)$$

$$2CuO + CO \rightarrow Cu_2O + CO_2 \quad (2)$$

$$CuO + CO \rightarrow Cu + CO_2 \quad (3)$$

$$2C + O_2 \rightarrow 2CO \quad (4)$$

$$C + O_2 \rightarrow CO_2 \quad (5)$$

$$CO + \frac{1}{2}O_2 \rightarrow CO_2 \quad (6)$$

$$C + H_2O \rightarrow CO + H_2 \quad (7)$$

$$CO + H_2O \rightarrow CO_2 + H_2 \quad (8)$$

$$C + CO_2 \rightarrow 2CO \quad (9)$$

$$Cu_2O + CO \rightarrow 2Cu + CO_2 \quad (10)$$

$$Cu_2O + C \rightarrow 2Cu + CO \quad (11)$$

2. Materials and Methods

2.1 Oxygen carrier preparation. Two different Cu-based oxygen carriers were prepared using physical mixing and incipient wetness impregnation (IWI) methods. In both oxygen carrier samples, the support/inert medium was Al_2O_3 (Sigma-Aldrich, fused powder, primarily α-phase, 74-149 μm). The Al_2O_3 was added to limit agglomeration of the CuO particles and improve fluidization in the reactor. Pure CuO (Sigma-Aldrich, 99.99% trace metals basis, powder) was used for the physically mixed (abbreviated from this point on as "Mixed") oxygen carrier. Studies have shown that as CuO content is raised the particles comprising a reaction mixture are more likely to agglomerate,[20,21] leading to loss of fluidization and greatly inhibiting the CLC process. Pure CuO particles sinter at temperatures as low as 800° C,[22] but an ore containing 44 wt% CuO exhibited only slight sintering after 5 reduction-oxidation cycles at 900° C with no defluidization observed.[21] In this study, the Mixed carrier contained 20wt% CuO/Al_2O_3. The metal oxide and Al_2O_3 were thoroughly mixed by stirring the dry powder until the CuO loading appeared uniform.

Another study by de Diego et al.[18] showed that when a dry impregnation technique is used to deposit 10 wt % of CuO onto the surface of an Al_2O_3 support, no agglomeration of the carrier material was observed after 20 reduction-oxidation cycles at temperature of 950° C. Therefore, in this study IWI samples underwent impregnation with a copper nitrate solution until the CuO loading reached approximately 9wt% CuO/Al_2O_3. The CuO loading above 9wt% CuO/Al_2O_3 decreased significantly after successive impregnations and as a result 9wt% CuO/Al_2O_3 was chosen for reduction testing in this study. Details of the oxygen carrier sample preparation were previously reported.[17] To approximate the porosity and specific area of the reduced oxygen carriers, CuO was calcined under N_2 purge for 1 hour at 1000° C to form Cu_2O used in BET analyses discussed later in this work. Pure CuO and Cu_2O were subjected to BET analysis. Pure component BET surface area and porosity is needed to calculate effectiveness factor η for reactions 2, 3, and 10. In these reactions Al_2O_3 is an inert and its presence could distort the surface area and porosity calculated from BET measurements.

2.2 Coal char preparation. The coal sample used in this study was a sub-bituminous coal obtained from the U.S. Department of Energy's National Carbon Capture Center (NCCC). It was obtained from the Powder River Basin (PRB) in Wyoming USA. The coal was sieved to obtain a particle size of 106-180 μm. Proximate analysis results for the raw PRB coal sample, obtained using ASTM D7582, are given in Table 1. Coal char was prepared by pyrolyzing the PRB coal at 950°C. The coal was pyrolyzed under continuous flowing N_2 for approximately 1 hour. This procedure was repeated twice to remove all volatile species. After pyrolysis, the PRB char sample contained 87.74% fixed carbon and 12.26% ash.

Table 1. Proximate analysis of the PRB coal, and PRB char generated at 950°C.

	wt%			
	Moisture	Volatile	Fixed Carbon	Ash
PRB Coal (As Received)	3.34	44.64	45.64	6.38
PRB Char	-	-	87.74	12.26

2.3 Drop Tube Fluidized Bed Reactor (DT-FBR). The reduction kinetics of the oxygen carrier with PRB coal char were studied using a drop tube fluidized bed reactor (DT-FBR). A schematic of the DT-FBR unit is shown in Figure 3. The reactor tube was clear fused quartz 25 mm outside diameter x 19 mm inside diameter x 122 cm length. The bottom of the fluidized bed was supported by a porous support made of a stainless-steel screen covered in high-temperature Al_2O_3/refractory fiber insulation wrap. The reactor tube mounted vertically in a 3-zone Lindberg/Blue M tube furnace (max T=1200°C) with a total heated length of 61 cm. The temperature inside the reaction tube was monitored by a K-type thermocouple positioned under the porous bed support at the bottom of the fluidized bed. Oxygen carrier bed fluidization was done by introducing a sweep gas (Ar, 99.999%) at the bottom of the reactor. The gas flow rate was controlled by an Alicat Scientific mass flow controller.

First, the reactor was purged with Ar gas by venting out the top of the reactor through the purge valve. The oxygen carrier and coal char samples were thoroughly mixed to the desired char:oxygen carrier mass ratio (C:O) prior to loading into the reactor. Ideally, all the oxygen released from the carrier leaves the reactor as CO_2 instead of toxic CO. Thus the stoichiometric ratio is 1 mole C to 2 moles O. From Equation 1, 4 moles of CuO (318 grams) are necessary for the release of 1 mol O_2, or 2 mol O. Because the PRB coal char is only ~88 wt% C (Table 1), 13.6 grams of PRB char is needed to supply the 1 mole C (12 grams) to react with the released O_2. Thus, the stoichiometric C:O ratio defined in units of mass is 13.6:318, or 0.043:1. To clarify the effect of the C:O ratio on the outlet gas and reduced carrier compositions, in this work the C:O ratio was varied from 0 to 0.30. With the drop valve closed, carrier and char were loaded into the reactor, sitting on the drop valve. The sweep gas kept the reactor purged of air while loading the sample through the purge valve. The reactor temperature was increased to the desired set-point (850°C-1100°C) for each test. Once the reactor temperature reached a steady-state, the drop valve was opened, allowing the oxygen carrier and coal char to drop into the reactor and land on the porous bed support. Because the carrier/char mixture heats rapidly after being dropped into the DT-FBR, the reaction takes place at roughly isothermal conditions. The gas concentrations (Ar, O_2, CO and CO_2) from the exit stream were measured with a Pfeiffer OmniStar GSD 301 quadrupole mass spectrometer (QMS).

Over the range of temperatures (850-1100° C) and sphericity (0.65-1) of interest, the CuO, Al_2O_3, a composite particle modeling the IWI carrier of 9 wt% CuO/91% Al_2O_3, and coal char were found to have the following minimum fluidization velocities: 1.44-2.21 cm/s, 0.59-0.90 cm/s, 0.63-0.97 cm/s and 0.70-1.08 cm/s, respectively. The range of these values depends on the sphericity of the particles calculated between 0.65-1. The actual flow rate of gas entering the tube ranged from 18.4 cm/s at 850° C and 22.5 cm/s at 1100° C. The distribution of particles with different minimum fluidization velocities ensured adequate mixing and fluidization of the oxygen carrier bed. This range of velocity values more than ensures that all particles of varying sphericity in the bed are fluidized at 850-1100° C, ensuring adequate mixing. The gas moves through the tube quickly: based on a heated reactor length of 80 cm, the residence time of gas in the reactor was found to range between 3.56-4.35 sec as the temperature increased from 850-1100 ^{o}C.

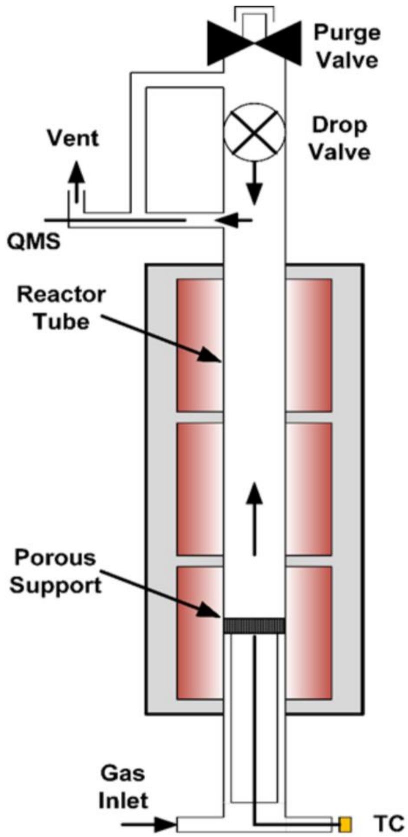

Figure 3. Schematic of the drop tube fluidized bed reactor (DT-FBR).

2.4. XRD. X-ray diffraction (XRD) analysis was carried out using a PANalytical X'Pert PRO multipurpose diffractometer equipped with a Cu anode operated at 45 kV and 40 mA and a divergent beam monochromator. Samples were ground in a corundum mortar and pestle before analysis. Data was collected under ambient conditions. Phase identification was verified by comparison to the International Centre for Diffraction Data (ICDD) inorganic compound data base.

2.5. SEM. An FEI Quanta 450 scanning electron microscope (SEM) with an Oxford Instruments X-MaxN 50 energy dispersive X-ray analyzer was used to investigate the morphology and particle size distribution of the oxygen carriers. The samples were mounted on conductive tape on an aluminum planchet and were not coated prior to analysis. Low vacuum mode was used to compensate for sample charging. An accelerating voltage of 20 kV and a working distance of about 10 mm were used to examine the sample particles in backscattered electron mode.

2.6. Test Matrix. The process conditions used in this study were the same as previously reported testing without coal char.[17] Oxygen carrier reduction tests were carried out in the DT-FBR on the Mixed (20wt% CuO/Al_2O_3) and IWI (9wt% CuO/Al_2O_3) carriers. A Cu_2O Mixed (18wt% Cu_2O/Al_2O_3) carrier was also produced by reduction of the Mixed carrier with no coal char present at 900° C; this Cu_2O Mixed carrier was produced solely to investigate the tendency of coal char to cause reduction of Cu_2O to Cu metal. It was not feasible to easily produce IWI carriers with 20 wt% CuO/Al_2O_3.[17] Reduction kinetics were measured with an Ar sweep flow of 1.0 SLM (standard Liter per minute) and a feed mass of 1.0-2.0 g. A sensitivity study of these process variables showed that an Ar flow rate of 1.0 SLM and a total feed mass of at least 1.0 g was necessary for minimizing the percentage of sample that was carried out of the reactor while also maintaining a high enough $CO/CO_2/O_2$ concentration in the exit gas stream for QMS analysis.[17] The reactor temperature was varied between 850°C-1100°C. Various C:O feed ratios ranging from 0.019-0.30 were tested to determine the optimum C:O ratio for kinetic analysis; for these experiments the feed mass was 2 g. The mixture was held at reaction temperature until the signals for CO, CO_2, and O_2 each fell below the detection threshold. For lower C:O feed ratios of 0.019-0.075 the reaction time was ~300 s, but reaction time rose to 3000 s for C:O feed ratio of 0.30. Process conditions for the experiments conducted in this work are summarized in Table *2*. For the kinetic analysis discussed in Section 3.1, a relatively low C:O ratio of 0.075 was chosen to limit undesired CO production from the combustion and gasification reactions while also keeping O_2 concentration near zero as a result of char combustion. For these experiments, a feed mass of 1 g was chosen to maximize the heating rate and ensure that the experiment proceeded at approximately isothermal conditions. The oxygen carrier reduction kinetics were evaluated from the product gas concentrations measured by QMS exiting the reactor. The form of the reduced carrier (Cu_2O/Cu) was determined from XRD and SEM analyses performed on solid samples removed from the reactor.

Table 2. Test matrix details for experiments performed in this work.

Reaction Time (s)	C:O Ratio	Temperature (°C)	Carrier
260	0.019	900	Mixed
350	0.038	900	Mixed
500	0.075	900	Mixed
3000	0.30	900	Mixed
3000	0.30	900	Cu_2O Mixed
2500	0.30	1000	Cu_2O Mixed
2500	0.30	1100	Cu_2O Mixed
300	0.075	850	Mixed
300	0.075	900	Mixed
300	0.075	950	Mixed
300	0.075	1000	Mixed
300	0.075	1050	Mixed
300	0.075	1100	Mixed
300	0.075	850	IWI
300	0.075	900	IWI
300	0.075	950	IWI
300	0.075	1000	IWI

300	0.075	1050	IWI
300	0.075	1100	IWI

3. Results and Discussion

3.1 Effect of PRB Char Addition on Reduced Carrier Composition and Structure. Depending on the degree of reduction, the oxygen carrier material may be present as either CuO, Cu_2O or Cu. In one study, metallic Cu was shown to be the primary reduced phase in a CuO-based carrier material, which exhibited severe particle agglomeration and ultimately led to defluidization and loss of carrier effectiveness.[23] The total percentage of CuO present in the raw carrier was 60 wt%. However, agglomeration and defluidization at CLC conditions where CuO reduction down to Cu metal is possible have been avoided in part by ensuring that the CuO content of the raw carrier material does not exceed 10 wt%.[18] Micrographs obtained using SEM indicate that the raw Mixed carrier is comprised of aggregates of small, micron-sized CuO particles [Figure 4a]. Cu-based species are marked by light regions in the micrographs, while the larger, darker particles represent Al_2O_3. No change to particle size or structure was observed upon reduction of the raw Mixed carrier to Cu_2O at 900° C for 300 seconds (Figure 4b), and XRD results tabulated in Table 3 indicate that no Cu metal formation was observed at these reaction conditions. To determine the effect of char addition on Cu_2O at elevated temperatures, the reduced Mixed carrier (defined as Cu_2O Mixed to distinguish it from the CuO-based Mixed carrier) shown in Figure 4b was subsequently mixed with PRB char at a large char loading of C:O = 0.30 and held at 900° C for 3000 s. As indicated in Figure 4c, many of the small, micron-sized particles comprising the Cu_2O aggregates observed in Figure 4b agglomerated to form considerably larger particles, although some of the original aggregates remained. The reaction product was mostly Cu metal (Table 3). If the Cu_2O is reacted with the char at 1100° C instead of 900° C with C:O = 0.30, Figure 4d indicates that the only Cu-based species in the reaction product is now Cu metal. After the reaction, the Cu-based species existed mainly in the form of spherical globules, not aggregates of small, micron-sized particles (Cu metal melts at 1084° C).

The likelihood of defluidization increases as agglomerate size grows larger. Given the demonstrated propensity of heavy char loadings to cause formation of agglomerates even in mixtures containing only 18 wt% Cu_2O, the effect of a lower C:O ratio of 0.075 on the particle size and structure of the reaction product was investigated. Both the Mixed and IWI carriers were reduced at C:O = 0.075 for 300 seconds at both 850° C and 1100° C. From Table 3, all reduction products are mostly comprised of Cu_2O with only a small amount of Cu metal present. The reaction of CuO and Al_2O_3 to form both $CuAl_2O_4$ and $CuAlO_2$ is thermodynamically favored in the temperature range used in this study. However, neither was observed in the XRD results in this work or a previous study by this research group.[17] Possible reasons that these species are not detected include: (1) the kinetics of the solid-solid reaction to form $CuAl_2O_4$ and $CuAlO_2$ are sufficiently slow that detectable amounts of these species do not appear after ~ 5 minutes in the reactor, and (2) the relatively low calcination temperature (900° C) of the IWI carrier.[17] Indeed, previous work[18] indicates that the potential for aluminate formation increases with calcination temperature at 950° C or higher, or for large number of reduction/oxidation cycles. Even the IWI carrier, which initially consists of CuO deposited onto the surface of low-porosity Al_2O_3, likely exhibits insufficient contact between CuO and Al_2O_3 for detectable formation of $CuAl_2O_4$ and $CuAlO_2$ within the reactor residence times considered in this study. Even though Cu metal is present, no sintering or agglomeration of partic les was observed in the reduced Mixed or IWI carriers [Figure 4e and Figure 4g] after reduction at 850° C. Only some very small agglomerates are observed in the reduced Mixed and IWI carriers [Figure 4f and Figure 4h] after reduction at 1100° C. It appears that defluidization is minimal even at 1100° C for moderate char loadings. Therefore, a C:O ratio of 0.075 was used for the kinetic comparison experiments described in this work.

Table 3. Characterization of reduced carrier materials at various C:O, temperature and initial carrier composition. For all reductions, the flow rate of Ar purge gas was 1 SLM.

Carrier	Active Metal Oxide	Support	C:O	T (°C)	Major XRD Peaks	Minor XRD Peaks	Major Gas Species
Mixed	20 wt% CuO	80 wt% Al_2O_3	0	900	Al_2O_3, Cu_2O	None	O_2
Cu_2O Mixed	18 wt% Cu_2O	80 wt% Al_2O_3	0.30	900	Al_2O_3, Cu	Cu_2O	CO, CO_2
Cu_2O Mixed	18 wt% Cu_2O	80 wt% Al_2O_3	0.30	1100	Al_2O_3, Cu	None	CO, CO_2
Mixed	20 wt% CuO	80 wt% Al_2O_3	0.075	850	Al_2O_3, Cu_2O	Cu	CO_2
Mixed	20 wt% CuO	80 wt% Al_2O_3	0.075	1100	Al_2O_3, Cu_2O	Cu	CO_2
IWI	9 wt% CuO	91 wt% Al_2O_3	0.075	850	Al_2O_3, Cu_2O	Cu	CO_2
IWI	9 wt% CuO	91 wt% Al_2O_3	0.075	1100	Al_2O_3, Cu_2O	Cu	CO_2

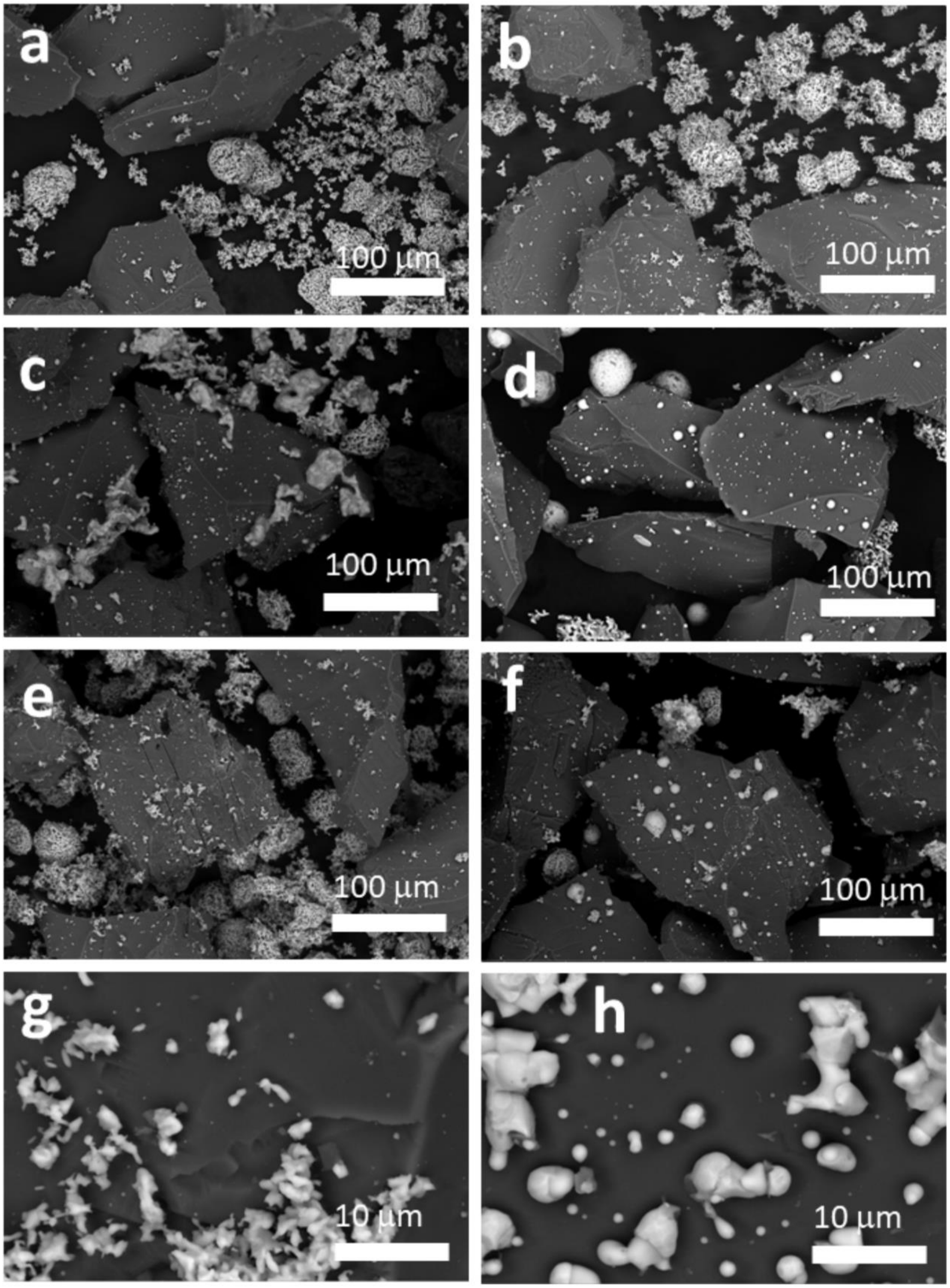

Figure 4. SEM micrographs of (a) raw Mixed carrier, (b) Mixed carrier reduced at 900°C, C:O = 0, 18 wt% Cu_2O/Al_2O_3 carrier reduced at (c) 900° C and (d) 1100° C, Mixed carrier reduced at

C:O = 0.075 and temperatures of 850° C (e) and 1100° C (f), IWI carrier reduced at C:O = 0.075 and 850° C (g) and 1100° C (h).

3.2 CFD Model. A kinetic model is necessary for elucidation of the effect of temperature and C:O ratio on both overall kinetic rate of CuO reduction and the formation of Cu metal in both the Mixed and IWI oxygen carriers in the presence of PRB char. To incorporate the effects of particle fluidization and heating rate of the dropped sample on the reaction rates, a computational fluid dynamics (CFD) program was used in this work. The software used was the MFiX-TFM (Multiphase Flow with Interphase Exchanges – Two Fluid Model) code designed at NETL (version 2016.1) and it is available at https://mfix.netl.doe.gov/mfix/download-mfix/. This code was designed particularly for systems involving fluid flow around particles. It is also convenient because of the ease of writing user-defined subroutines to describe system-specific characteristics, such as kinetic rate laws. Within MFiX-TFM, fluids and solids are represented as interpenetrating continua within a Eulerian-Eulerian model. To simplify modeling calculations, a single average particle size 140 μm was assumed. This composite particle was comprised of Al_2O_3, CuO, carbon, and ash. Further information about the system modeled is given in Table 4. The kinetic equations given in Table 5 were incorporated into a user-defined subroutine that is added to the MFiX-TFM coding.

While the composite CuO/Al_2O_3/C/ash particle assumption is not a strict representation of the situation of the Mixed or IWI carriers in the reactor, minimum fluidization velocity values for CuO, Al_2O_3, the IWI carrier, and C are on the same order of magnitude. The range of particle sizes and sphericity values help to ensure that the bed contents are well-mixed. Thus, the composite particle assumption could provide at least a rough approximation of the fluidization behavior of the Mixed carrier particles and char. When the average solid packing fraction in the reactor is at least ~0.25 (moderate fluidization), contact between the solids (most importantly, char and CuO/Cu_2O) should be substantial at a given time. Necessarily, these particles must touch if this solid-solid reaction is to occur. For substantially lower solid packing fraction values, the use of the composite particle assumption is not recommended.

Table 4. Reactor dimensions and experimental conditions for CFD model.

Property	Value
Reactor height	80 cm (160 cells)
Reactor inside diameter	2 cm (6 cells)
Minimum void fraction	0.50
Reactor pressure	1.2 bar
Ar purge gas flow rate	1.0 SLM
Average composite particle size	140 μm
Reactor temperature	850, 900, 950, 1000, 1050, 1100° C
Initial sample temperature	27° C
Maximum time step size	0.0008-0.001 s

C:O feed ratios were 0.019, 0.038, 0.075, and 0.30. The initial CuO content of the oxygen carrier (no carbon or ash present) was 9 wt % (for IWI) or 20 wt % (for Mixed). Values for intrinsic reaction rate constant k_r are given in Table 5 for Reactions 1-11, along with the associated rate laws. The conditions under which external and/or internal diffusional limitations to mass transfer must be considered are discussed in detail in Section A.1 and Figure S1 of the Supporting Information.

In Table 5, the rate constants $k_{r1,mixed}$, $k_{r1,LI}$, k_{r2}, k_{r3}, and k_{r10} are in s^{-1}; k_{r4} and k_{r5} are given in cm/s; k_{r6} has units of $(cc/mol)^{0.8}*s$; $k_{r7,1}$ and $k_{r9,1}$ are in $mol^{1/3}/(bar*s*cc^{1/3})$; $k_{r7,2}$ and $k_{r9,2}$ are in bar^{-1}; k_{r8} has units of $mol/(cm^3*bar^2*s)$; k_{r11} has units of $cm^3/mol/s$. All rate expressions are in units of $mol/(cm^3*s)$. Reactions 6 and 8 are homogeneous gas-phase reactions. Preliminary calculations indicated that Reactions 1, 7, 9, and 11 proceeded slowly enough such that the intrinsic reaction rate was orders of magnitude slower than external diffusion. Internal diffusion was not a hindrance, as effectiveness factor η approached 1. Therefore, for reactions 1, 6, 7, 8, 9, and 11, the intrinsic reaction rate constants in the left-hand column of Table 5 were determined to be equal to the apparent rate constant and were thus used in the rate expression in the right-hand column of Table 5. However, in reactions 2, 3, and 10, internal diffusion limitations to the rate of reaction cannot be neglected so the effectiveness factor η is incorporated in the corresponding rate expression in Table 5. Finally, in reactions 4 and 5, limitations to apparent reaction rate constants k_4 and k_5 from both internal and external diffusion cannot be neglected. The values for k_4 and k_5 must be calculated from the intrinsic rate constants kr_4 and kr_5 given in Table 5 using the procedure explained in Section A.1 of the Supporting Information. All bracketed variables, such as char concentration [C], have units of mol/cm^3. The variables P_{O2}, P_{H2O}, P_{CO}, P_{CO2}, and P_{H2} represent, in units of bar, the partial pressures of oxygen, water, carbon monoxide, carbon dioxide, and hydrogen. In Equations 4 and 5, ε_c represents the volume fraction occupied by char particles.

Table 5. Rate laws and values of intrinsic reaction rate constant k_r for Reactions 1-11.

Reaction	k_r (Intrinsic)	Reactor	Rate Expression	Ref.

1	$k_{r1,mixed} = 25.8e^{-\frac{80500}{RT}}$ $k_{r1,IWI} = 249.7e^{-\frac{98900}{RT}}$	Fluidized bed	$r_{1,mixed} = 0.75k_{1,mixed}[CuO]^{\frac{2}{3}}[CuO]_0^{\frac{1}{3}}\theta$ $r_{1,IWI} = 0.75k_{1,LI}[CuO]^{\frac{2}{3}}[CuO]_0^{\frac{1}{3}}\theta$ $\theta = \left(1 - \frac{P_{O_2}}{P_{O_2,eq}}\right)^{0.333}$	17
2	$k_{r2} = 3.76E10e^{-\frac{90000}{RT}}$	Fluidized bed	$r_2 = \eta k_{r2}[CO]\left(\frac{[CuO]}{[CuO]_0}\right)^{\frac{2}{3}}$	24
3	$k_{r3} = 1.4E6e^{-\frac{28000}{RT}}$	Fluidized bed	$r_3 = \eta k_{r3}[CO]\left(\frac{[CuO]}{[CuO]_0}\right)^{\frac{2}{3}}$	24
4, 5	$k_{r4} = 2.22E6e^{-\frac{169000}{RT}}$ $P = \left[\frac{CO}{CO_2}\right] = 2512e^{-\frac{51900}{RT}}$ $k_{r5} = 4.44E4e^{-\frac{144000}{RT}}$	Entrained flow	$r_4 = \frac{P}{P+1}k_4[O_2]\left(\frac{\varepsilon_c}{1-\varepsilon_c}\right)$ $r_5 = \frac{2}{P+1}k_5[O_2]\left(\frac{\varepsilon_c}{1-\varepsilon_c}\right)$	25,26
6	$k_{r6} = 1.20E11e^{-\frac{66900}{RT}}$	Stirred reactor	$r_6 = k_{r6}[CO][O_2]^{0.3}[H_2O]^{0.5}$	27
7	$k_{r7,1} = 11441e^{-\frac{116154}{RT}}$ $k_{r7,2} = 2.56e^{\frac{4116}{RT}}$	Fluidized bed	$r_7 = \frac{k_{r7,1}P_{H_2O}}{1 + k_{r7,2}P_{H_2O}}[C]^{\frac{2}{3}}$	28
8	$k_{r8} = 17.93e^{-\frac{4895}{RT}}$	----------	$r_8 = k_{r8}\left[P_{CO}P_{H_2O} - \frac{P_{CO_2}P_{H_2}}{K_{WGSR}}\right]$ $K_{WGSR} = 10^{-2.42+0.000386T+\frac{2181}{T}}$	26,29
9	$k_{r9,1} = 175200e^{-\frac{152130}{RT}}$ $k_{r9,2} = 1.87e^{\frac{6236}{RT}}$	Fluidized bed	$r_9 = \frac{k_{r9,1}P_{CO_2}}{1 + k_{r9,2}P_{CO_2}}[C\}^{\frac{2}{3}}$	28
10	$k_{r10} = 9.6E7e^{-\frac{56000}{RT}}$	Fluidized bed	$r_{10} = \eta k_{r10}[CO]\left(\frac{[Cu_2O]}{[Cu_2O]_0}\right)^{\frac{2}{3}}$	24
11	$k_{r11} = 283e^{-\frac{9967}{T}}$	Fluidized bed	$r_{11} = \frac{0.5k_{r11}[C][Cu_2O]}{\left\{\left(\frac{[Cu_2O]_0}{[Cu_2O]}\right)^{\frac{1}{3}} - 1\right\}}$	This work

The intrinsic rate constant k_2 for Reaction 2 is intrinsically very fast at 850-1100° C. However, the carrier material must be very porous or the reaction rate is limited by internal pore diffusion.[24] Because the Cu_2O formed from the reaction of CuO and CO (Reaction 2) subsequently reacts with CO to form metallic Cu (Reaction 10), it is not possible to observe Reaction 2 in isolation. Therefore, from existing literature results it may only be possible to estimate the intrinsic reaction rate constant k_2 and therefore the kinetic constants of Arrhenius prefactor and activation energy. Chuang et al.[24] establish a lower bound of 80 kJ/mol for the activation energy for Reaction 2, $2CuO + CO \rightarrow Cu_2O + CO_2$. In addition, microscopy results taken from a reaction sample collected at 800° C indicate a substantial ratio of Cu_2O to metallic Cu during the early stages of reaction. These results suggest that at elevated temperature (above 800° C) the rate of Reaction 2 is at least one order of magnitude higher than that of the competing reaction $CuO + CO \rightarrow Cu + CO_2$ which is defined as Reaction 3 herein. In this work, it was determined that for Reaction 2, an Arrhenius prefactor of 3.76E10 and activation energy of 90000 J/mol provided the best fit to model data.

Kinetics for the CO-forming combustion and gasification of coal char depend greatly upon the type of parent coal from which the coal char was derived. The combustion rate can be expressed as $r = k_c(P_{O2})^n$. However, the order of combustion with respect to oxygen partial pressure P_{O2} can vary for different types of coal char. Depending on the parent coal from which a char is derived, the intrinsic combustion rate at 1 atm O_2 can vary by up to three orders of magnitude.[30] Therefore, kinetics for combustion reactions 4 and 5 are derived from an expression determined specifically for PRB coal char. In addition, the apparent kinetic constants for gasification vary greatly with respect to the type of coal from which the char studied was derived, with variation from 45-200 kJ/mol not uncommon for the activation energy of Reaction 9.[31]

It is necessary to account for the H_2O-catalyzed oxidation of CO (Reaction 6) and steam gasification (Reaction 7) because of the desorption of water from the dropped sample upon heating. The desorption of water can be approximated as temperature-independent for the range of temperatures considered in this work. From analysis of H_2O detected in the gas eluting from the DT-FBR, the rate of water desorption $r_{H_2O,desorb} = 0.0636C^2/C_0$, where C and C_0 represent the current and initial H_2O concentrations (mol/cm^3) in the cell and C_0 corresponding to 0.14% (mass) of the original carrier being comprised of adsorbed H_2O.

Various kinetic expressions for Reaction 6 are available in the literature.[32,33] A common feature in these works is the finding that, although not consumed during the reaction, H_2O is necessary as a catalyst for Reaction 6. Most of these studies were carried out at or near atmospheric pressure, at CO, O_2 and H_2O partial pressures significantly higher than those encountered in the drop tube reactor used in this study. Howard et al.[33] compiled results from more than a dozen investigations spanning 567-2087°C, to obtain a global kinetic relationship. However, there was a substantial amount of scatter in the data depending on the investigation; more than an order of magnitude might lie between experimental and predicted rate constant. Because the kinetic expression of Hottel et al.[27] was derived from experiments conducted at partial gas pressures as low as 0.25 atm, this expression was chosen as even lower gas partial pressures were encountered (typically no higher than 0.04 atm for CO, CO_2, or O_2) in this work.

Kinetics of the gasification reactions depend greatly on the properties of the coal from which the char was derived; therefore, in this work kinetics were used for the steam and CO_2 gasification of PRB coal char calculated from experiments performed in the same laboratory. Typically, coal char gasification follows the shrinking core model.[34,35,36] However, kinetic relationships that are first-order in char composition have also been proposed.[37] The rate constant for Reaction 9 (CO_2 gasification) has been expressed in the form of a Langmuir-Hinshelwood model,[38, 39] as this model provided the best representation of rate constant over the dynamic CO_2 pressure range (0.0001 to 0.1 bar) encountered in the reactor in this work. A similar model was used for steam gasification, Reaction 7. Experimental data used to obtain the kinetic relationships for the gasification reactions were obtained at NETL and are available elsewhere.[28]

Prior experiments in our laboratory indicate that Cu_2O does not react in the presence of Ar, even at elevated temperature. It was demonstrated in Section 3.1 that, when heated to 900-1100° C in the presence of Ar purge gas at 1.0 SLM, the Mixed Cu_2O and C react in a solid-solid reaction to form Cu metal, CO_2 and CO. Because C does not undergo reaction at even the elevated temperatures of 900°C-1100°C in the presence of Ar, it is proposed that first Cu_2O and C react to form Cu metal and CO gas via Reaction 11. The evolved CO then provides the fuel for Cu_2O reduction by Reaction 10.

The temperature dependence of the kinetic rate constant k_{11} for Reaction 11 was determined in the following manner. The Cu_2O Mixed carrier was mixed with PRB char at C:O = 0.30 at reaction temperatures of 900°C, 1000°C, and 1100°C. The DT-FBR was held at the specified reaction temperature until both CO_2 and CO responses from the QMS had fallen below the detection threshold. The variation with respect to time of the overall extent of Cu_2O conversion $X_{red,Cu2O}$ in terms of moles of oxygen released was calculated from the CO_2 and CO elution curves (no O_2 was detected) as prescribed in Equation 15. As indicated in Figure 5, $X_{red,Cu2O}$ can be resolved into two terms X_{10} and X_{11} representing the individual extents of Cu_2O conversion via Reactions 10 and 11, respectively.

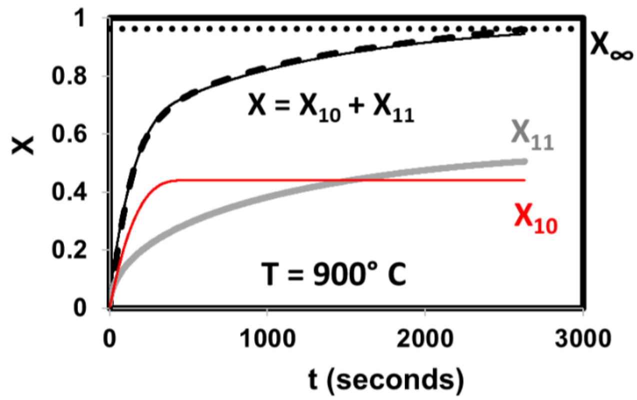

Figure 5. Three predicted curves of conversion as a function of time during the isothermal reaction of Cu_2O with elemental C (PRB C:O ratio 0.30). Curve $X_{10}+X_{11}$: a summation of parallel reactions given by Curves X_{10} and X_{11}. Dotted markers represent the experimental overall extent of reaction $X_{red,Cu2O} = X_{10} + X_{11}$.

The following equation was used to fit the experimental data for extent of Cu_2O reduction $X_{red,Cu2O}$ in a manner similar to Monazam et al.,[40] who used the equation obtained from Velisaris and Sefeis[41] to resolve the observed extent of Cu_2O reduction $X_{red,Cu2O}$ into a function of the two individual extents of Cu_2O reduction given by X_{10} and X_{11}.

$$\frac{X_{red,Cu2O}}{X_\infty} = w_{10}X_{10}(t) + w_{11}X_{11}(t) \qquad (12)$$

Above, $X_{red,Cu2O}$ represents the overall extent of Cu_2O reduction as a function of time, t; X_∞ represents the overall extent of reaction at the conclusion of all reactions and is obtained from mass spec gas elution data; w_{10} and w_{11} represent the weights of Reactions 10 and 11 ($w_{10} + w_{11} = 1$), and X_{10} and X_{11} in Figure 5 and Equations 12-14 represent the extents of Reactions 10 and 11 as a function of time t. X values representing reduction of Cu_2O to metallic Cu were determined from the mass balance and from total moles of O (from CO, CO_2, or O_2) detected by the quadrupole mass spectrometer (QMS) according to Equation 15. The values of the fitting parameters k'_{10} and k'_{11} are related to X_{10} and X_{11} as follows:

$$1-(1-X_{10})^{\frac{1}{3}}=k'_{10}t \quad (13)$$

$$1+2(1-X_{11})-3(1-X_{11})^{\frac{2}{3}}=k'_{11}t \quad (14)$$

Equation 13 is calculated by rearranging the expression for r_{10} in Table 5 as a function of X_{10} instead of [Cu_2O]. Because the concentration of CO varies over the course of the Cu_2O reduction, the parameter k'_{10} does not reflect the value of the true rate constant k_{10} and is therefore distinct from the true rate constant k_{10} referenced in Table 5. Thus, the parameter k'_{10} is not used in any of the CFD calculations in this work. Equation 14 obeys the ash diffusion kinetic model, which holds for many solid-solid reactions and was therefore selected to model the solid-solid reaction of Cu_2O and C. It was not possible to express Equation 14 as an explicit function $X_{11}(t)$. Therefore, it was necessary to utilize a computer program to solve for the value of X_{11} iteratively. Values for w_{11}, k'_{10} and k'_{11} were determined iteratively for each reaction temperature by minimizing the difference between the value of $X_{red,Cu2O}$ calculated from Equation 12 and the experimental value obtained using QMS data and Equation 15. They are given in Table 6. Values for ln k'_{11} are plotted against 1/T and given in Figure 6. The rate constant k'_{11} must be manipulated to account for the char concentration [C]. The expression for the true rate constant k_{11} for Reaction 11 is determined by first assuming that the rate of Reaction 11 is first order with respect to char concentration [C], and then by dividing the expression for k_{11}' given in Figure 6 by [C] such that $k'_{11}=k_{11}$[C]. The use of a large excess of char (C:O = 0.30) for these calculations ensured that the concentration of char could be approximated as constant for the purposes of calculating k_{11} for Reaction 11. The average concentration [C] of char C in the volume in which Reaction 11 occurs was estimated to be 0.005 mol/cc. This value was estimated from the known mass and weighted mass average density of CuO, Al_2O_3, and char loaded into the reactor, and from the average after solid fraction predicted from simulation. (0.12 g C initially present)*(1 mol C/12 g C)*(average 0.25 solid fraction at reaction conditions)*(4.4 g/cc)/(2.13 g total mass loaded to reactor) = 0.005 mol/cc.

Table 6. Experimentally obtained values for fitting parameters in Equations 12-14.

	Temperature (° C)		
C:O = 0.30	900	1000	1100
X_∞	0.96	1.00	0.99
w_{11}	0.543	0.23	0.147
k'_{10}	0.0021	0.0065	0.015
k'_{11}	0.00029	0.00056	0.0010

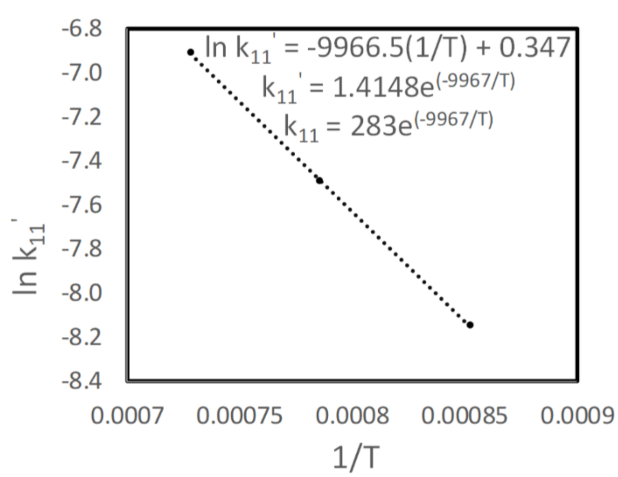

Figure 6. For a C:O ratio of 0.30, the value of k_{11}' is calculated for reduction of Cu_2O to Cu metal.

3.3. Determination of Overall CuO Oxygen Carrier Reduction Kinetics. Reduction kinetic parameters for solid oxygen carriers in the presence of PRB char are needed for the design of CLC reactor systems. The apparent overall reduction kinetic parameters of activation energy E_A and Arrhenius pre-exponential factor A for both the Mixed and IWI CuO oxygen carriers in the presence of PRB char were calculated over a temperature range of 850°C-1100°C, as indicated in Table 7 and Figure 7. To determine E_A and A, it is first necessary to calculate the apparent overall CuO reduction rate constant $k_{ov}(T)$ for both carriers at each reaction temperature. For the calculation of $k_{ov}(T)$, *it is* first necessary to know the extent of conversion X as a function of time. Because the purge gas entering the reactor is 99.999% Ar, all the oxygen in the product gas is assumed to come from reduction of the carrier. The X for the oxygen carrier reduction is defined in Equation 15,

$$X = \frac{n_O(t)}{n_{O,f}} \tag{15}$$

where $n_O(t)$ is the cumulative number of moles of oxygen detected in all oxygen-containing product gases up to time t. The parameter $n_{O,f}$ is the cumulative number of moles of oxygen detected in all oxygen-containing product gases up to the time the reaction is complete. Values of $n_O(t)$ and $n_{O,f}$ were determined from eluting gas compositions obtained using a QMS calibrated for quantitative measurement of O_2, CO and CO_2 in Ar.

To determine the kinetic parameters of the oxygen carrier reduction reaction under Ar in the presence of coal char, several experiments were conducted at different temperatures (850°C, 900°C, 950°C, 1000°C, 1050°C and 1100°C). The reduction of CuO in the presence of coal char is a complicated process as several different reactions occur simultaneously, and CuO, Cu_2O or Cu may be present depending on the degree of reduction at various reaction temperatures. However, if both over-reduction of Cu_2O to metallic Cu and the direct reduction of CuO to metallic Cu represent less than ~10% of the total oxygen released, then almost all oxygen released is associated with CuO reduction to Cu_2O. In such a scenario, apparent kinetic parameters may be approximated for the overall reduction of CuO to Cu_2O as if it were a single, composite reaction. The rate of change of conversion with respect to reaction time (*dX/dt*) may be used to describe the oxygen carrier reduction rate. The general reaction rate can be written in terms of the reaction model *f(X)* and $k_{ov}(T)$ (Equation 16).

$$\frac{dX}{dt} = k_{ov}(T)f(X) \tag{16}$$

Based on a previous study of the reduction of CuO-based oxygen carriers without coal char,[17] a Shrinking Sphere Model (3-D contraction) produced the best fit of the reduction data. In this work, the Shrinking Sphere model also provided the best fit to the data for reduction of the oxygen carrier in the presence of PRB char. For the Shrinking Sphere Model, $f(X) = 3(1 - X)^{2/3}$, the apparent overall CuO reaction rate constant $k_{ov}(T)$ follows the Arrhenius relationship which is given in Equation 17,

$$k_{ov}(T) = Aexp\left(^{-E_A}/_{RT}\right) \tag{17}$$

where A is the Arrhenius pre-exponential factor, E_A is the activation energy and R is the universal gas constant. To determine $k_{ov}(T)$ at a particular set of reaction conditions, the variables in Equation 16 are separated while setting $f(X) = 3(1 - X)^{2/3}$. Subsequent integration yields Equation 18. If experimental values for extent of reaction X are known, then a plot of $1 - (1 - X)^{1/3}$ versus time t can be used to determine the value of the rate constant, $k_{ov}(T)$. A discussion and sample calculation indicating how the CO, CO_2, and O_2 gas elution curves were ultimately used to calculate X and the experimental $k_{ov}(T)$ at 900° C and C:O = 0.075 is given in the Supporting Information and is illustrated in Figures S2 and S3.

$$1 - (1 - X)^{\frac{1}{3}} = k_{ov}(T)t \tag{18}$$

In Figure 7, experimental kov(T) values for the reduction of both the 20wt% CuO/Al_2O_3 physically mixed and 9wt% CuO/Al_2O_3 IWI carriers in the presence of PRB char at C:O = 0.075 are shown on Arrhenius plots for temperatures of 850° C, 900° C, 950° C, 1000° C, 1050° C, and 1100° C. The goal of this kinetic analysis was to evaluate the kinetic parameters of CuO reduction with PRB char and compare these results to the parameters without coal char. Experimental values of $k_{ov}(T)$ for the same Mixed and IWI carriers with no char present and at the same temperatures were obtained from Means et al.[17] and are also plotted in Figure 7. The slope of the Arrhenius plots in Figure 7 for both the physically mixed and IWI carriers without char present is non-linear at temperatures below ~950° C where the O_2 uncoupling reaction (Equation 1) is thermodynamically limited. Oxygen uncoupling from CuO is an equilibrium reaction and the thermodynamics of the forward reaction favor high temperature and low O_2 gas concentration. The equilibrium O_2 partial pressure associated with the CuO/Cu_2O system is discussed in greater detail in our previous work.[17] If O_2 is consumed by combustion with coal char, Le Chatelier's principle predicts that further reaction will occur as equilibrium shifts in the direction of more Cu_2O product. Indeed, when C:O = 0.075, the Arrhenius plots in Figure 7 derived from experimental data are almost linear for both samples as the equilibrium oxygen uncoupling limitations are overcome through the char combustion of oxygen. At 850° C, the effect of char addition is to increase the value of $k_{ov}(T)$ more than threefold for both Mixed and IWI carriers. With PRB coal char in the feed (C:O = 0.075) and in the temperature range of 950°C-1100°C, the experiments indicated only somewhat increased $k_{ov}(T)$ values for both carriers relative to those measured without char present in the reactor. As the temperature approached 1100°C, the difference between the reaction rate with and without coal char decreased greatly. The near convergence of these data sets at 1100°C suggest that the reaction rates aren't equilibrium-limited at this temperature.

Also examined in Figure 7 is the ability of the CFD model to reproduce $k_{ov}(T)$ for CuO reduction at these conditions. A sample validation of CFD model predictions against experimental data for CO_2, CO, and O_2 gas composition is shown in the Supporting Information in Figure S4. CFD model predictions for X, obtained from the predicted gas elution data arising from reduction of both the Mixed and IWI carriers, are validated against experimental results in Figure S5. For these calculations, $k_{ov}(T)$ is obtained from X predictions from the CFD model by plotting $1 - (1 - X)^{\frac{1}{3}}$ versus time. The results in Figure 7 indicate that in most cases CFD predictions for $k_{ov}(T)$ agree with the experimentally determined value to within ±10%. This observation is true for both the physically mixed and the IWI carriers. Kinetic parameters of Arrhenius pre-exponential factor and activation energy for both the 20 wt% CuO/Al_2O_3 mixed carrier and the 9 wt% CuO/Al_2O_3 IWI carrier were derived from experimental $k_{ov}(T)$ and given in Table 7. Kinetic parameters for each carrier were also derived from the $k_{ov}(T)$ obtained from the CFD model and are given in Table 7.

Table 7. Kinetic parameters for apparent overall rate of CuO reduction derived from extent of reaction data obtained from both experiment and CFD.

Material	A (min^{-1})	E_a (kJ/mol)
20 wt% CuO Mixed (C:O = 0)[17]	1550	80.5
20 wt% CuO Mixed (C:O = 0.075)	804	72.1
20 wt% CuO Mixed CFD (C:O = 0.075)	873	72.0
9 wt% CuO IWI (C:O = 0)[17]	15000	98.9
9 wt% CuO IWI (C:O = 0.075)	1020	68.4

9 wt% CuO IWI CFD (C:O = 0.075)	1310	70.4

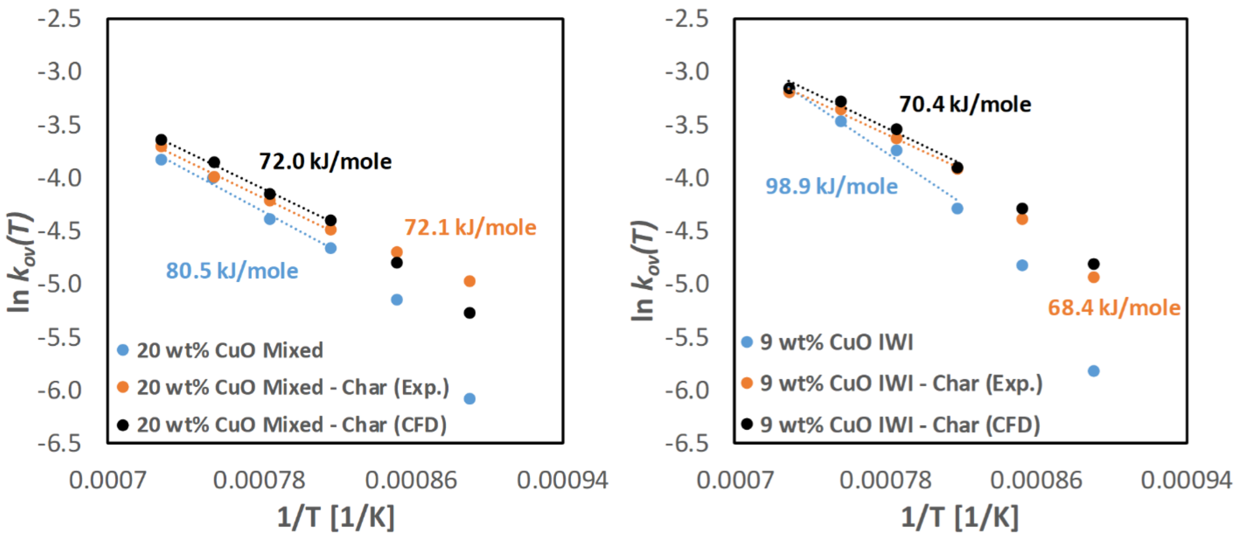

Figure 7. CFD is able to accurately model $k_{ov}(T)$, when char is present (C:O = 0.075) for both the Mixed and IWI carriers.

3.4. Effect of C:O Ratio on Reaction Time and Cu Metal Formation. CFD simulation was used to obtain an understanding of how C:O ratio and temperature affect the production of Cu_2O, CO, and Cu metal. From the rate equations given in Table 5, these overall rates are defined as follows:

$$r_{Cu2O} = 2r_1 + r_2 - r_{10} - r_{11} \tag{19}$$

$$r_{Cu} = r_3 + 2r_{10} + 2r_{11} \tag{20}$$

The overall rate of Cu_2O formation, r_{Cu2O}, incorporates CuO reduction from oxygen uncoupling via Reaction 1 as well as an additional pathway of CuO reduction by CO in Reaction 2. The overall rate of Cu formation, r_{Cu}, encompasses unwanted CuO reduction by CO, unwanted Cu_2O reduction by CO and unwanted Cu_2O reduction by solid C char via Reactions 3, 10, and 11 respectively.

CFD simulation was first used to investigate the effect of PRB char on r_{Cu2O} by increasing the rate of the CLOU reaction, r_1. According to Figure 7, the addition of char (C:O = 0.075) to the CuO/Al_2O_3 carrier effects an increase in the overall rate of Cu_2O formation at all temperatures from 850° C to 1100° C. However, the increase in value of the overall CuO reduction rate constant $k_{ov}(T)$ is much more pronounced at the lower temperatures of 850° C and 900° C than at the higher temperatures of 950-1100° C. At 850° C, Figure 7 indicates that addition of PRB char at C:O = 0.075 triples the kinetic rate for reduction of both the Mixed and IWI carriers. This behavior suggests that the reduction of CuO is thermodynamically limited at 850° C, and to a somewhat lesser extent, at 900° C. According to Table 5, the kinetic rate constants $k_{1,mixed}$ and $k_{1,LI}$ for the CLOU reduction of the CuO comprising the Mixed and IWI carriers are both a function of $\theta = \left(1 - \frac{P_{O_2}}{P_{O_{2,eq}}}\right)^{0.333}$, which ranges from 0 to 1. The larger the value of $\frac{P_{O_2}}{P_{O_{2,eq}}}$, the lower the value of θ and the more thermodynamically limited the CLOU reduction is. This ratio represents the partial pressure of oxygen P_{O2} divided by the equilibrium partial pressure of oxygen $P_{O2,eq}$. At 900° C, $P_{O2,eq}$ is only 0.014 bar. However, $P_{O2,eq}$ rises with respect to temperature, causing θ to rise. At 950° C, the rising value of θ has overcome most of the equilibrium limitations to oxygen uncoupling even when no char is added and at 1050° C $\theta \sim 1$ at all reaction times (Figure 8). In the case of C:O = 0 and 900° C, Figure 9a indicates that the value of P_{O2} stays near 0.010 bar for much of the reaction time. At these conditions, the value of θ is only 0.66 (Figure 9b). According to Figure 9a, the C:O ratio must be increased to at least 0.075 if P_{O2} is to be sufficiently minimized such that it exerts a negligible slowing effect on $k_{1,mixed}$ and $k_{1,LI}$. At these conditions, the maximum value of $\frac{P_{O_2}}{P_{O_{2,eq}}}$ is about 0.15, occurring at a time of about 40 seconds. Therefore, at C:O = 0.075, the value of θ is always above 0.95 and further increases in C:O ratio will effect only a very limited improvement in the rate of the CLOU reaction. Indeed, Figure S6 in the Supporting Information indicates that the rate of O_2 uncoupling via the CLOU reaction (Reaction 1) rises rapidly as C:O ratio is increased from 0 to 0.075. However, it plateaus above C:O = 0.075, and the maximum CLOU reaction rate at the significantly higher C:O = 0.30 is almost identical to that observed at C:O = 0.075.

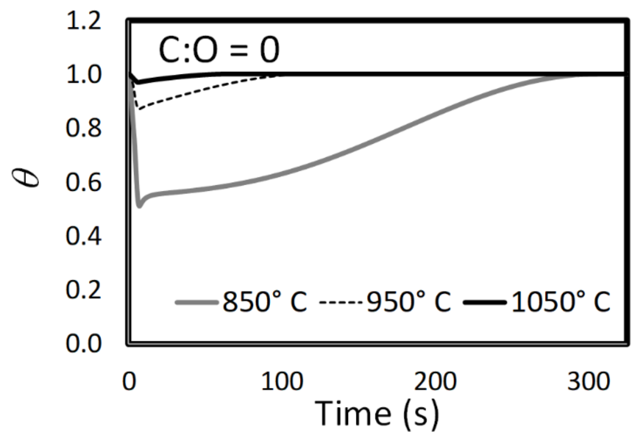

Figure 8. Variation of θ with respect to reduction time.

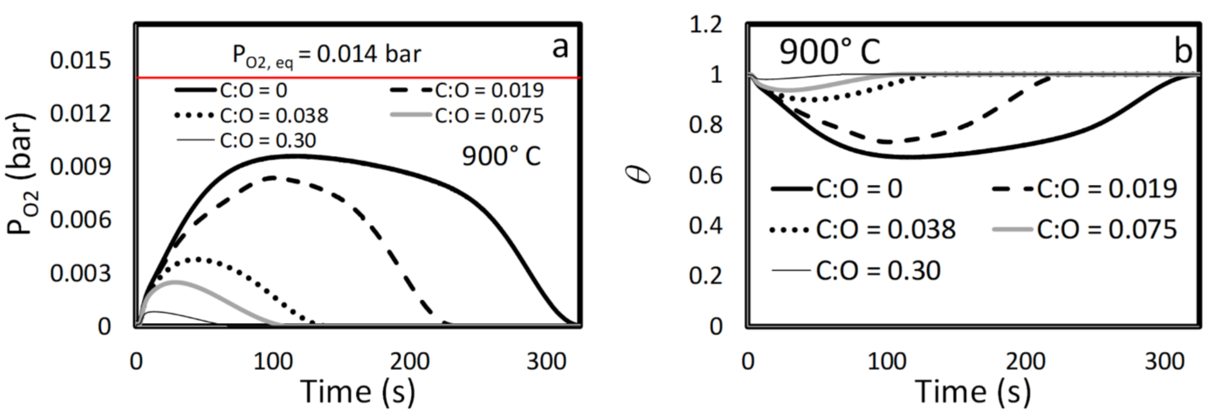

Figure 9. (a) Predicted equilibrium partial pressure P_{O2} and (b) θ for C:O ratios 0-0.30 at 900° C.

It is apparent from the results in Figure 9 that the addition of PRB char removes thermodynamic barriers to the CLOU reduction of CuO by the combustion of O_2. Unfortunately, combustion of O_2 results in the formation of CO. The presence of CO not only makes an alternate pathway to Cu_2O formation possible (Reaction 2), but also opens a pathway for the unwanted reduction of both CuO and Cu_2O to metallic Cu (Reactions 3 and 10). As discussed previously in Section 3.1, the relatively low melting point of metallic Cu (1084° C) greatly facilitates agglomeration and loss of effectiveness of CuO-based oxygen carriers. Clearly it is beneficial to know the conditions under which $\frac{r_{Cu_2O}}{r_{Cu}}$ is maximized. As indicated in Figure 10, the CFD model predicts that $\frac{r_{Cu_2O}}{r_{Cu}}$ is maximized at C:O = 0.038. These predictions are consistent with the experimental observations of previous investigators,[14,21] who used relatively small C:O ratios to ensure operation of CLC at conditions with excess O_2 to ensure complete combustion of fuel to form CO_2.

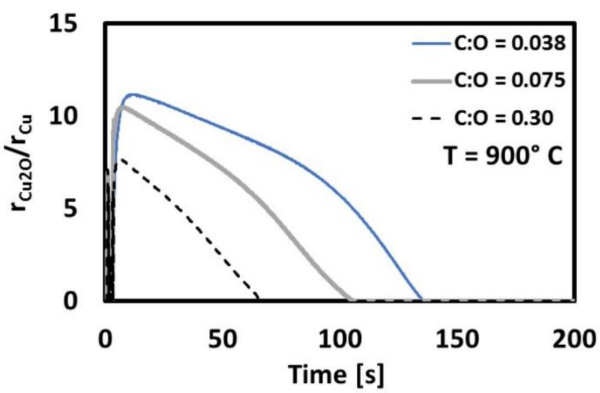

Figure 10. Ratio of Cu_2O production rate to Cu metal at various C:O loadings.

Next, a study was performed to determine the extent to which Cu production could be limited by controlling reaction time during reduction of the Mixed carrier, particularly at C:O ratios much higher than 0.038. As indicated in Figure 11a, the reaction time at 900° C for a C:O ratio of 0.038 is 125 seconds. As most of the PRB char is consumed in the combustion of O_2, Cu formation was minimal after the CLOU reaction concluded at about 125 seconds. The Cu metal composition at C:O = 0.038 was lower than the XRD detection threshold of ~1 wt % and does not appear in the

XRD diffraction pattern (Figure 11d) of the corresponding sample, which was taken after the full reaction time of 350 seconds. Increasing C:O ratio to 0.075 reduced the reaction time to 100 seconds (Figure 11b) and after the reaction was concluded at 500 seconds Cu was detected in the diffraction pattern (Figure 11e). A further increase in C:O ratio from 0.075 to 0.30 lowered the predicted CuO reaction time to 63 seconds. Figure S7 in the Supporting Information indicates that increased char gasification rate is the primary reason for the decrease in reaction time from 100 seconds at C:O = 0.075, to 63 seconds at C:O = 0.30. The char combustion rate leveled off above C:O = 0.075 but the char gasification rate increased from a negligible value at C:O = 0.038, up to about half the char combustion rate when C:O = 0.30. The additional CO increased the CuO reduction rate by CO (Reactions 2 and 3) until it was greater than the rate of CuO reduction by CLOU (Figure S6).

However, as C:O ratio was increased, there was a corresponding increase observed in the predicted Cu mass fraction, x_{Cu} at the time the CuO reaction was complete – first to 0.012 for C:O = 0.075, and then to 0.017 for C:O = 0.30. The over-reduction of Cu_2O to Cu metal was particularly pronounced at C:O = 0.30 (Figure 11c). Ultimately the CFD kinetic model predicted that for a C:O ratio of 0.30, nearly all of the Cu_2O is reduced to Cu metal at a reaction time of 3000 seconds. This finding was qualitatively confirmed via the XRD diffraction pattern in Figure 11f. The higher char loading of C:O = 0.30 greatly increased the rate of Cu_2O reduction by coal char (Reaction 11), ensuring the continued production of CO even after the CLOU reaction was complete and no O_2 was present. The CO reduces Cu_2O (Reaction 10), producing Cu metal and CO_2. Increases in char loading resulted in a corresponding increase in the rate at which this CO_2 was gasified by char to produce more CO (Reaction 7) for reaction with Cu_2O. However, at all C:O ratios the extent of Cu metal formation and subsequent particle agglomeration can be greatly curtailed by ensuring that

x_{CuO} does not fall below ~0.10, limiting CuO conversion to no more than 50%. A previous study[18] indicated that when conversion is constrained to no more than 50%, CuO/Al_2O_3 oxygen carriers can be re-used for many reduction-oxidation cycles without agglomeration.

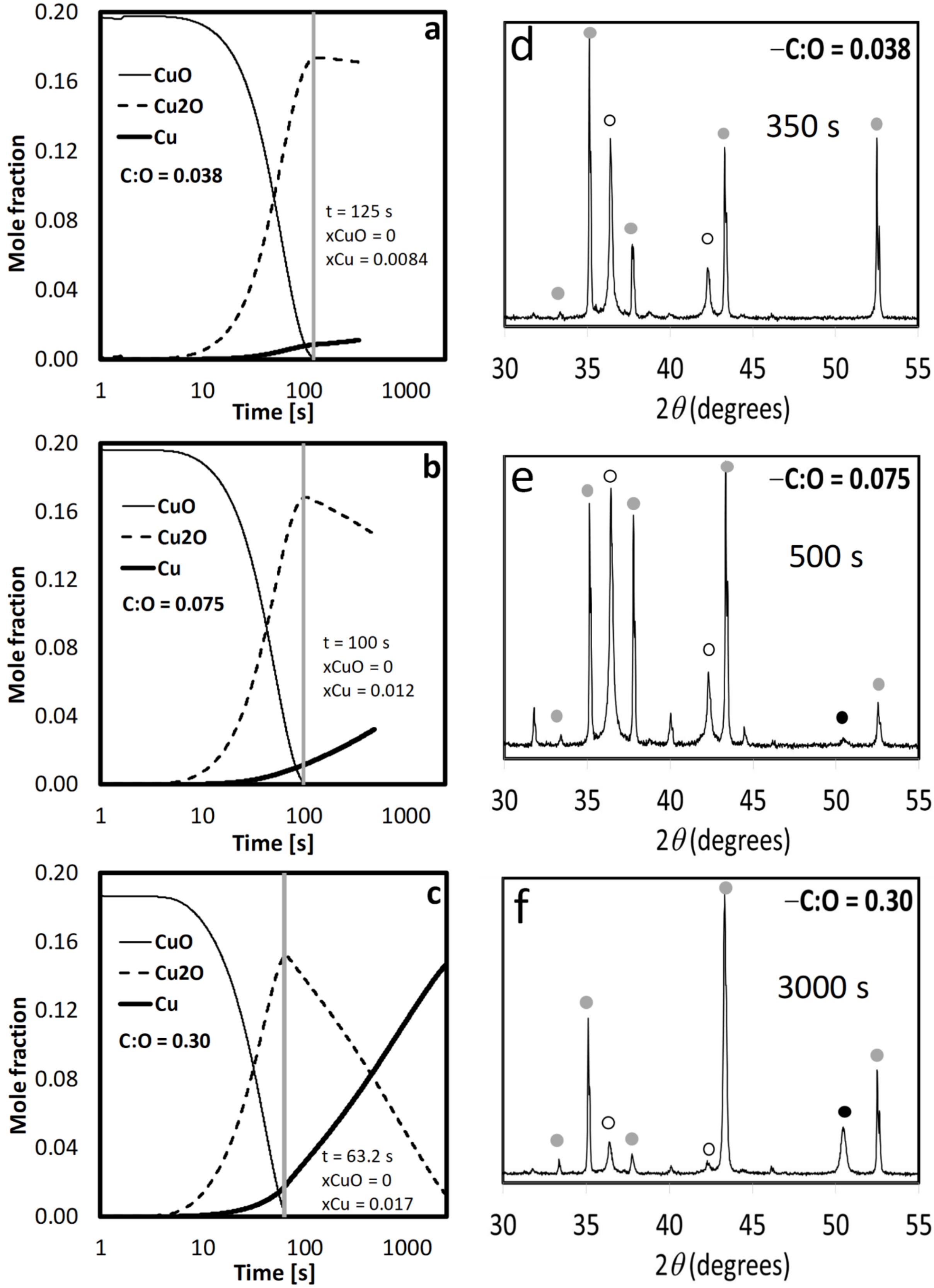

a
CuO
Cu2O
Cu
C:O = 0.038
t = 125 s
xCuO = 0
xCu = 0.0084
b
C:O = 0.075
t = 100 s
xCuO = 0
xCu = 0.012
c
C:O = 0.30
t = 63.2 s
xCuO = 0
xCu = 0.017
Mole fraction
Time [s]
d
C:O = 0.038
350 s
e
C:O = 0.075
500 s
f
C:O = 0.30
3000 s
2θ (degrees)

Figure 11. Predicted composition profiles for reduction of Mixed CuO/Al_2O_3 carrier at 900° C at C:O ratios of (a) 0.038, (b) 0.075, (c) 0.30. The corresponding XRD diffraction patterns are given in panels (d), (e), and (f). Gray circles – Al_2O_3, White circles – Cu_2O, Black circles – Cu metal.

3.5. Effect of Temperature on Reaction Time and Cu Metal Formation. In a study of how temperature influences reaction time and Cu metal formation, the carrier composition profiles with respect to reaction time were also predicted for both the Mixed and IWI carriers at a C:O ratio of 0.075 and temperatures of 850° C and 1100° C (Figure 12). For both carriers, reaction temperature had a negligible effect on final value of x_{Cu}. At 1100° C production rate of CO through gasification should be much greater than that at 850° C. However, temperature clearly had a negligible effect on the propensity for Cu to form. While the respective activation energies for CO_2 and H_2O gasification are relatively high at 152 kJ/mol and 116 kJ/mol, the respective activation energies for the reduction of CuO and Cu_2O by CO are only 28 kJ/mol and 56 kJ/mol (modest in comparison to the activation energy for CuO reduction by oxygen uncoupling given in Figure 7 and Table 5). The low activation energies for the reductions of CuO and Cu_2O by CO to form Cu lead to only a modest increase in the respective rate constants k_3 and k_{10} for these reactions and appeared to cancel out any gain in reaction rate from increased CO production. Even then, CO composition in the purge gas was negligible. At this low C:O = 0.075, the maximum CO_2 concentration in the purge gas was ~5.5% by volume (Figure S4a in Supporting Information). The initial CO response was below the detection threshold of 0.01% but after the CuO reduction time of 22 seconds passed, the CO response increased to a maximum of only 0.05% by volume (Figure S4b in Supporting Information). CFD prediction at 1100° C was almost a perfect match for the experimentally determined CO_2 concentration with respect to time for the physically mixed sample (Figure S4a).

In addition, CFD predictions were close for the corresponding CO and O_2 elution curves (Figures S4b and S4c). Finally, because of the lower 9 wt% starting composition of CuO, the final values of x_{Cu} in the IWI carrier were proportionally lower.

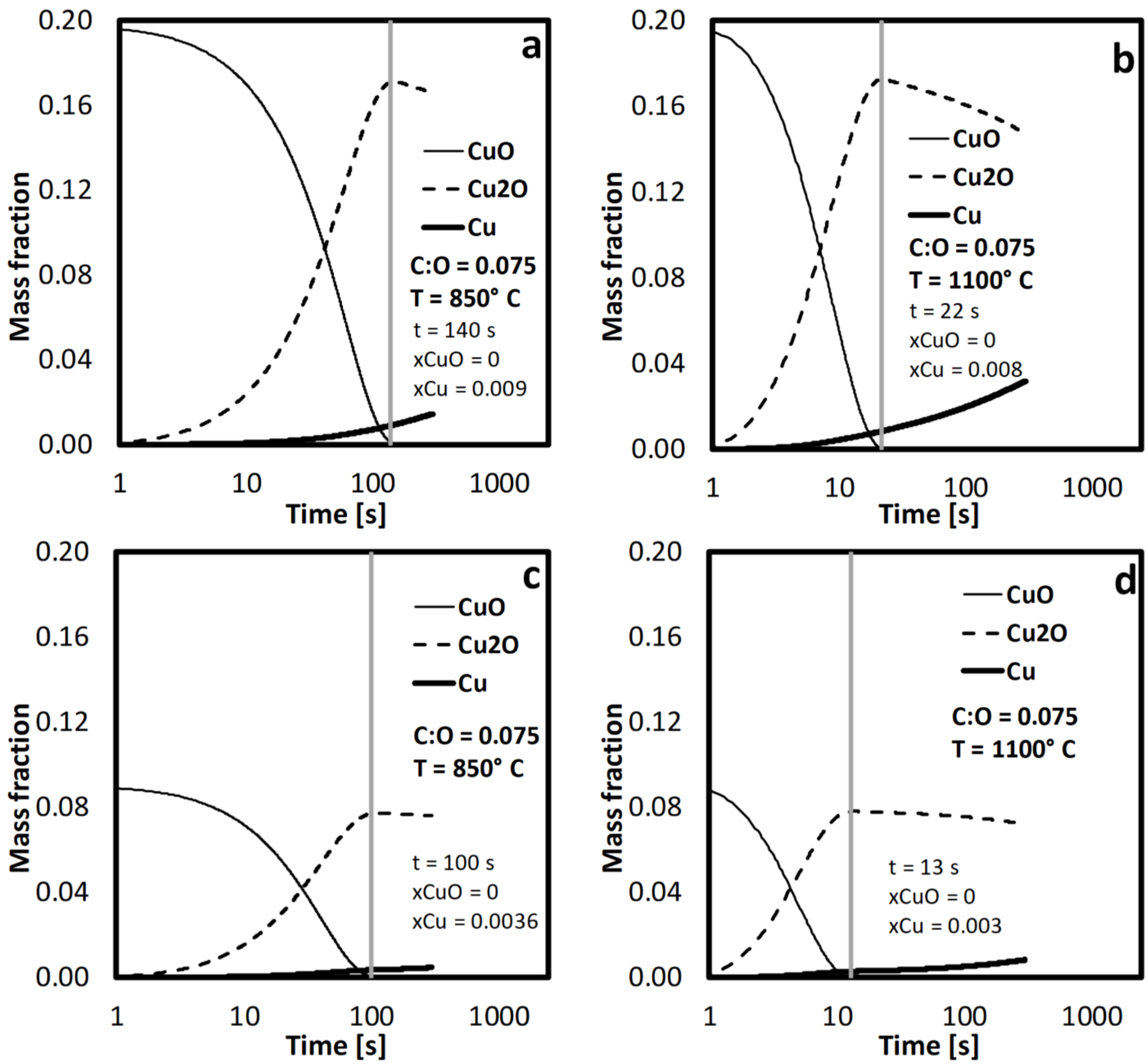

Figure 12. Predicted composition profiles for the Mixed carrier at (a) 850° C and (b) 1100° C, and for the IWI carrier at (c) 850° C and (d) 1100° C.

4. Conclusions

A 20wt% CuO/Al_2O_3 CLOU carrier was prepared by physical mixing, and a 9wt% CuO/Al2O3 sample was prepared using incipient wetness impregnation. Although multiple reactions contribute to the reduction of CuO at C:O = 0.075, a single Shrinking Sphere kinetic model accurately described the overall reduction of both carriers. The overall CuO reduction rate constant $k_{ov}(T)$ of both oxygen carriers mixed with coal char derived from PRB coal were determined experimentally at near-isothermal conditions using a DT-FBR at reaction temperatures from 850°C to 1100°C. Results for $k_{ov}(T)$ were compared to those obtained with only carrier and no char present. The CFD model showed promise as a simulation tool for the reduction of CuO in the presence of coal char, as it yielded comparable predictions for apparent overall CuO reduction rate constant $k_{ov}(T)$ that are typically within 10% of the experimental value (Figure 7). To the best of the authors' knowledge, this work represents the first in which an accurate multi-reaction kinetic model has been validated for the reduction kinetics for the system of CuO + solid fuels.

The CFD model was used to predict the effect of char loading and temperature on the CuO reduction time and Cu metal formation. The model confirmed that the addition of a very small amount of C (C:O = 0.075) causes combustion of the uncoupled O_2, all but eliminating the thermodynamic limitations to the CLOU reaction (Reaction 1) even at temperatures as low as 850° C where the equilibrium constant is only 0.004. At 850° C, the addition of PRB char at C:O = 0.075 caused a tripling of the kinetic rate. Conversely, the observed increase in the kinetic rate was considerably less pronounced at 1100° C, where the equilibrium constant of the CLOU reaction is much larger. At temperatures above 950°C, equilibrium limitations to oxygen uncoupling are small even when char is not present. The CFD model confirmed that the addition of PRB char also resulted in CO formation through combustion and gasification reactions, raising the observed $k_{ov}(T)$ by opening an alternative pathway to Cu_2O production. Virtually all the increase in kinetic rate at 1100° C was a result of this alternative pathway to Cu_2O production. However, the presence of CO was also shown to open an undesired reaction pathway to Cu metal formation.

The reduction of CuO required only 63 seconds at 900° C when a large excess of PRB char (C:O = 0.30) was introduced to the reactor. This reaction time is an order of magnitude faster than that typically encountered during the gasification-limited reduction of Fe_2O_3. However, tight control of reaction time is necessary to prevent massive over-reduction of the Cu_2O to metallic Cu. The use of a much lower C:O ratio of 0.038 increased the reaction time to 125 seconds. In this case there was much less potential for Cu metal formation at any reaction time because there was less C present and therefore less CO produced.

Acknowledgment

This work was performed in support of the US Department of Energy's Fossil Energy Crosscutting Technology Research Program. The Research was executed through the NETL Research and Innovation Center's Advanced Combustion – CLC Field Work Proposal. Research performed by Leidos Research Support Team staff was conducted under the RSS contract 89243318CFE000003.

Disclaimer

This project was funded by the Department of Energy, National Energy Technology Laboratory, an agency of the United States Government, through a support contract with Leidos Research Support Team (LRST).

Supporting Information

The Supporting Information is available free of charge on the ACS Publications website.

Mass Transfer Calculations (Section A.1)

Sample Calculation for Overall CuO Reduction Rate Constant $k_{ov}(T)$ (Section A.2)

Validation of Kinetic Model (Section A.3)

Variation of O_2 Uncoupling, CO Reduction of CuO, Combustion and Gasification Reaction Rates with Respect to C:O Ratio (Section A.4)

References

(1) Arrhenius, S. and E.S. Holden, On the influence of carbonic acid in the air upon the temperature of the earth. *Publ. Astron. Soc. Pac.* **1897**, *9(54)*, 14-24.

(2) Lewis, W.K.; Gilliland, E. R. Production of Pure Carbon Dioxide. US Patent 2665972A, 1954.

(3) Ishida, M.; Jin, H. A New Advanced Power-Generation System Using Chemical-Looping Combustion. *Energy* **1994**, *19*, 415-422.

(4) Lyngfelt, A.; Leckner, B.; Mattisson, T. A Fluidized-Bed Combustion Process with Inherent CO_2 Separation; Application of Chemical-Looping Combustion. *Chem. Eng. Sci.* **2001**, *56*, 3101-3113.

(5) Ishida, M., Jin, H.; Okamoto, T. A Fundamental Study of a New Kind of Medium Material for Chemical-Looping Combustion. *Energy Fuels* **1996**, *10*, 958-963.

(6) Leion, H.; Mattisson, T.; Lyngfelt, A. Solid Fuels in Chemical-Looping Combustion. *Int. J. Greenhouse Gas Control* **2008**, *2*, 180-193.

(7) Mattisson, T.; Lyngfelt, A.; Leion, H. Chemical-Looping with Oxygen Uncoupling for Combustion of Solid Fuels. *Int. J. Greenhouse Gas Control* **2009**, *3*, 11-19.

(8) Shen, L.; Wu, J.; Xiao, J.; Song, Q.; Xiao, R. Chemical-looping combustion of biomass in a 10 kW reactor with iron oxide as an oxygen carrier. *Energy Fuels* **2009**, *23*, 2498–2505.

(9) Adanez, J.; Abad, A.; Garcia-Labiano, F.; Gayan, P.; de Diego, L. F. Progress in Chemical-Looping Combustion and Reforming technologies. *Prog. Energy Combust. Sci.* **2012**, *38*, 215-282.

(10) Hossain, M.M.; de Lasa, H. I. Chemical-Looping Combustion (CLC) for Inherent CO_2 Aeparations - A Review. *Chem. Eng. Sci.* **2008**, *63*, 4433-4451.

(11) Leion, H.; Mattisson, T.; Lyngfelt, A. Using chemical-looping with oxygen uncoupling (CLOU) for combustion of six different solid fuels. *Energy Procedia* **2009**, *1*, 447–453.

(12) Siriwardane, R.; Tian, H.; Richards, G.; Simonyi, T.; Poston, J. Chemical-Looping Combustion of Coal with Metal Oxide Oxygen Carriers. *Energy Fuels* **2009**, *23*, 3885-3892.

(13) Adanez-Rubio, I.; Gayán, P.; Garcia-Labiano, F.; de Diego, L. F.; Adánez, J.; Abad, A. Development of CuO-Based Oxygen-Carrier Materials Suitable for Chemical-Looping with Oxygen Uncoupling (CLOU) Process. Energy Procedia **2011**, *4*, 417-424.

(14) Abad, A.; Adónez-Rubio, I.; Gayón, P.; García-Labiano, F.; de Diego, L. F.; Adánez, J. Demonstration of Chemical-Looping with Oxygen Uncoupling (CLOU) Process in a 1.5 kWth Continuously Operating Unit Using a Cu-Based Oxygen Carrier. *Int. J. Greenhouse Gas Control* **2012**. *6*, 189-200.

(15) Adánez-Rubio, I.; Gayán, P.; Abad, A.; García-Labiano, F.; de Diego, L. F.; Adánez, J. Kinetic Analysis of a Cu-based Oxygen Carrier: Relevance of Temperature and Oxygen Partial Pressure on Reduction and Oxidation Reactions Rates in Chemical Looping with Oxygen Uncoupling (CLOU). *Chem. Eng. J.* **2014**, *256*, 69-84.

(16) Zhou, Z.; Han, L.; Nordness, O.; Bollas, G. M. Continuous Regime of Chemical-Looping Combustion (CLC) and Chemical-Looping with Oxygen Uncoupling (CLOU) Reactivity of CuO Oxygen Carriers. *Appl. Catal. B*, **2015**. *166-167*, 132-144.

(17) Means, N. C.; Burgess, W. A.; Howard, B. H.; Smith, M. W.; Shekhawat, D. Reduction Kinetics and Behavior of Cu-Based Oxygen Carriers for Chemical-Looping with Oxygen Uncoupling (CLOU) in a Drop Tube Fluidized Bed Reactor. *Energy Fuels* **2019**, *33*, *6*, 5610-5619.

(18) de Diego, L.F.; Gayan, P.; Garcia-Labiano, F.; Celaya, J.; Abad, M.; Adanez, J. Impregnated CuO/Al_2O_3 Oxygen Carriers for Chemical-Looping Combustion: Avoiding Fluidized Bed Agglomeration. *Energy Fuels* **2005**, *19*, 1850–1856.

(19) Cao, Y.; Pan, W.-P. Investigation of chemical looping combustion by solid fuels. 1. Process analysis. *Energy Fuels* **2006**, *20*, 1836–1844.

(20) Wen, Y.-Y.; Li, Z.-S.; Xu, L.; Cai, N.-S. Experimental study of natural Cu ore particles as oxygen carriers in chemical looping with oxygen uncoupling (CLOU). *Energy Fuels* **2012**, *26*, 3919–3927.

(21) Zhao, H.; Wang, K.; Fang, Y.; Ma, J.; Mei, D.; Zheng, C. Characterization of natural copper ore as oxygen carrier in chemical-looping with oxygen uncoupling of anthracite. *Int. J. Greenhouse Gas Control* **2014**, *22*, 154–164.

(22) Ran, J.; Fu, F.; Qin, C.; Zhang, P.; Yang, L.; Wang, W.; Yang, L. Evaluation of $CuO/MgAl_2O_4$ in Biomass Chemical Looping Gasification with Oxygen Uncoupling. *BioResources* **2016**, *11(1)*, 2109-2123.

(23) Cho, P.; Mattisson, T.; Lyngfelt, A. Comparison of Iron-, Nickel-, Copper-, and Manganese-based Oxygen Carriers for Chemical Looping Combustion. *Fuel* **2004**; *83*, 1215-1225.

(24) Chuang, S. Y.; Dennis, J. S.; Hayhurst, A. N.; Scott, S. A. Kinetics of the Chemical Looping Oxidation of CO by a Co-Precipitated Mixture of CuO and Al_2O_3. *Proc. Comb. Inst.* **2009**; *32*, 2633-2640.

(25) Hecht, E. S.; Lighty, J. S.; Shaddix, C. R.; Kinetic Rates of Oxidation and Gasification Reactions of Coal Chars Reacting in Oxy-Combustion Environments. 8th US National Combustion Meeting. Paper 070CO-0309. May 19-22, 2013.

(26) Wen, C.Y.; Desai, P.R. Computer Modeling of Morgantown Energy Research Center's Fixed-bed Gasifier. Research report; Morgantown Energy Technical Center of U.S. Department of Energy; Morgantown, West Virginia (March 1978).

(27) Hottel, H. C.; Williams, G. C.; Nerheim, N. M.; Schneider, G. R. *Tenth Symposium (International) on Combustion*, p. 111, The Combustion Institute, 1965.

(28) Means, N. C.; Weiland, N. Kinetics and Simulation Comparisons of Char Gasification from Coal and Biomass Mixtures in CO_2 and Steam. 2013 ACS Spring National Meeting, New Orleans, LA.

(29) Wen, C. Y., 'Optimization of Coal Gasification Processes", R & D Research Report No. 66, Vol. 1 and 2 (1972).

(30) Smith, I. W. The Combustion Rates of Coal Chars: A Review. Nineteenth Symposium (International) on Combustion/The Combustion Institute, 1982, pp. 1045-1065.

(31) Liu, H.; Luo, C.; Kato, S.; Uemiya, S.; Kaneko, M.; Kojima, T. Kinetics of CO_2/char gasification at elevated temperatures Part I: Experimental results. *Fuel Proc. Tech.* **2006**, *87*, 775-781.

(32) Dryer, F. L.; Glassman, I. High-Temperature Oxidation of CO and CH_4. Fourteenth Symposium (International) on Combustion, The Combustion Institute, Pittsburgh, 987-1003.

(33) Howard, J. B.; Williams, G. C.; Fine, D. H. Kinetics of Carbon Monoxide Oxidation in Postflame Gases. Fourteenth Symposium (International) on Combustion, The Combustion Institute, Pittsburgh, 975-986.

(34) Osafune, K.; Marsh, H. Gasification kinetics of coal chars in carbon dioxide. *Fuel* **1988**, *67*, 384-388.

(35) Everson, R. C.; Neomagus, H. W. J. P.; Kasaini, H.; Njapha, D. Reaction kinetics of pulverized coal-chars derived from inertinite-rich coal discards: Gasification with carbon dioxide and steam. **Fuel** *2006*, *85*, 1076-1082.

(36) Ahn, D. H.; Gibbs, B. M.; Ko, K. H.; Kim, J. J. Gasification kinetics of an Indonesian sub-bituminous coal char with CO_2 at elevated pressure. *Fuel* **2001**; *80*, 1651-1658.

(37) Dutta, S.; Wen, C.; Belt, R. J. Reactivity of coal and char. 1. In carbon dioxide atmosphere. Ind. Eng. Chem. Proc. Des. Dev. **1977**, *16(1)*, 20-30.

(38) Kajitani, S.; Suzuki, N.; Ashizawa, M.; Hara, S. CO_2 gasification rate analysis of coal char in entrained flow coal gasifier. *Fuel* **2006**, *85*, 163-169.

(39) Huang, Z.; Zhang, J.; Zhao, Y.; Zhang, H.; Yue, G.; Suda, T.; Narukawa, M. Kinetic studies of char gasification by steam and CO_2 in the presence of H2 and CO. *Fuel Proc. Tech.* **2010**, *91*, 843-847.

(40) Monazam, E. R.; Breault, R. W.; Siriwardane, R.; Richards, G.; Carpenter, S. Kinetics of the reduction of hematite (Fe_2O_3) by methane (CH_4) during chemical looping combustion: A global mechanism. *Chem. Eng. J.* **2013**, *232*, 478-487.

(41) Velisaris, C. N.; Sefeis, J. C. Crystallization kinetics of polyetheretherketone (PEEK) matrices. *Polym. Eng. Sci.* **1986**, *26*, 1574-1581.